48th AIAA Aerospace Sciences Meeting Including the New Horizons Forum and Aerospace Exposition
4 - 7 January 2010, Orlando, Florida
AIAA 2010-652

Effects of Source Redistribution on Jet Noise Shielding

Salvador Mayoral* and Dimitri Papamoschou†
University of California, Irvine, CA 92697, USA

The potential of jet noise shielding from the Hybrid Wing Body (HWB) airplane is investigated in subscale experiments. The jet nozzle had a bypass ratio 10 and was operated at realistic takeoff exhaust conditions using helium-air mixtures. The shield, fabricated from a thin flat plate, had the generic shape of the HWB planform. Redistribution of the jet noise source is essential for achieving substantial noise reduction. Devices used to alter the jet noise source comprised chevrons (in mild and aggressive configurations) and a number of porous wedge fan flow deflectors. Using the estimated cumulative (downward plus sideline) EPNL reduction as a figure of merit, shielding of the plain nozzle yields a 2.4 dB reduction. Application of the aggressive chevrons increases the reduction to 6.5 dB, while the best wedge configuration improves this figure to 6.9 dB. Combination of wedge and aggressive chevrons yields a benefit of 7.6 dB. Examination of high-definition noise source maps shows a direct link between the insertion loss and the axial location of peak noise source. The aggressive chevrons cause an abrupt contraction of the noise source length at Strouhal number Sr=1.2, while the wedge induces a gradual contraction with increasing frequency. As a result, the insertion loss with the aggressive chevrons is stronger than with the wedge. However, because the wedge is inherently quieter than the chevrons, it gives a slightly better overall benefit. Surveys of the mean flow field show that the wedge, and its combination with chevrons, produces a significant reduction in the potential core length. On the other hand, the chevrons alone induce modest changes in the length of the high-speed region of the jet. Therefore, the mean velocity field by itself cannot provide useful information for inferring the noise source length for these complicated flows.

Nomenclature

D	=	nozzle exit diameter
f	=	frequency
M	=	Mach number
R	=	radius from nozzle plug tip to microphone
Sr	=	Strouhal number = fD_s/U_s
u	=	mean axial velocity in the jet plume
U	=	nozzle exit velocity
x, y, z	=	axial, transverse, and spanwise coordinates relative to plug tip.

Subscripts

p	=	primary (core) exhaust
s	=	secondary (fan) exhaust

I. Introduction

THIS study is motivated by the development of ultra-quiet advanced aircraft that shield engine noise with airframe surfaces. In such aircraft the engines would be mounted over-the-wing (OTW) to utilize the wing as a sound barrier between the emitted noise and the ground observer. The focus here is jet noise, which is particularly challenging to shield because the noise source is extended and directional. Significant experimental research on the OTW concept for conventional and short-takeoff airplanes occurred in the 1970s[1-3]. Important trends were established for the changes in the spectrum of acoustic emission versus shield parameters. However, the investigations were not extensive enough to develop reliable predictive tools. Commercially the OTW concept did not find support (with only one application, the rare and now extinct Fokker VFW614) and the research dried up.

Presently, the advent of the ultra-efficient Hybrid Wing-Body (HWB) airplane[4] has reinvigorated the OTW concept for jet noise shielding with its top-wing mounted engines. The HWB design in principle provides sufficient planform area to shield both the forward-emitting turbomachinery noise and the aft-emitting jet noise. Subscale

* Graduate Student Researcher, Department of Mechanical and Aerospace Engineering, smayoral@uci.edu. AIAA Student Member.
† Professor, Department of Mechanical and Aerospace Engineering, dpapamos@uci.edu, Fellow AIAA.

experiments in our laboratory were the first to assess the potential for the HWB planform to shield jet noise[5]. It was found that jet noise shielding was marginal unless the noise source was altered using devices such as chevrons or fan flow deflectors. Moving the unmodified nozzle upstream of its nominal position yielded small benefits. However, the aerodynamic penalty of placing the fan inlet in a near-sonic Mach number environment at cruise conditions will likely outweigh these benefits. Effective jet noise shielding therefore calls for the redistribution of the jet noise source using devices that will cause minimal aerodynamic loss. Candidate devices include chevrons and wedge-shaped perforated fan flow deflectors. The wedge-shaped deflectors, in the form of flaps, could be folded after takeoff to minimize performance penalties.

In this paper we extend our earlier work by optimizing the wedge fan flow deflector, investigating combinations of devices, surveying the jet noise source, and examining possible connections between the mean flow and the noise source distribution. We take advantage of recent enhancements of our facility that enable more robust acoustic surveys and more accurate detection of the jet noise source.

II. Experimental Details

A. Nozzle and shield configurations

Subscale jet noise shielding experiments were carried out with a nozzle–shield configuration composed of a dual-stream nozzle with an HWB-shaped shield, as depicted in Figs. 1 and 2. The scale factor was 90. The baseline nozzle is designed with a bypass ratio 10 and has a secondary (fan) diameter D_s =31.2 mm and fan exit height of 4.0 mm. The nozzle exit coordinates are plotted in Fig.3. The nozzle and its chevron counterparts were rapid-prototyped using high-definition stereolithography with a tolerance (layer thickness) of 0.178 mm. The HWB planform was manufactured from a 3.2-mm thick aluminum sheet preserving the essential dimensions for shielding. The shield features removable/adjustable verticals and an adjustable elevator flap. It was mounted on a longitudinal traverse that permits the axial displacement of the nozzle either upstream or downstream from its nominal position. For the experiments described here, the shielding configuration was "nominal" with the fan exit plane 2.27 fan diameters upstream of the trailing edge, the verticals at 79^o dihedral, and the elevator at zero deflection.

Nozzle modifications comprised chevrons and wedge-shaped fan flow deflectors. Two different sets of chevrons, designed by Boeing Co., were applied to the fan and core nozzles. The first, "mild" set of chevrons features 10 serrations with a 10° insertion angle. The second, "aggressive" set of chevrons features 10 serrations with a 20° insertion angle. Porous wedge fan flow deflectors of various geometries, listed in Table 1, were attached on the baseline BPR10 nozzle. A detailed investigation of porous wedge/flap fan flow deflectors can be found in Ref.6. The basic function of the wedge is to reshape the mean flow such that velocity gradients are reduced in the downward and sideline directions, hence reducing turbulent kinetic energy and sound generation in those directions. A porous wedge mitigates strong velocity gradients at the base of the wedge that can cause localized intense noise sources that can propagate to the far field. The wedges in this study were fabricated from a fine interwoven metal mesh with a mesh size of 0.0223 mm and porosity of 49.6%. Figure 4 shows the principal wedge and chevron configurations.

B. Aeroacoustic testing

The nozzles were attached to a dual-stream apparatus which delivers cold mixtures of helium and air to the primary (core) and secondary (bypass) nozzles. Helium-air mixtures have been shown to accurately duplicate the acoustics of hot jets[7]. The exit flow conditions, listed in Table 2, matched the typical exit conditions of a turbofan engine with bypass ratio 10 at takeoff power. The Reynolds number of the jet, based on fan diameter, was 0.68×10^6.

Noise measurements were performed in the aeroacoustic facility shown in Fig.5. The microphone array consists of twenty four 3.2-mm condenser microphones (Bruel & Kjaer, Model 4138). This is a significant enhancement to our previous setup that utilized only eight microphones[5]. For acoustic surveys, the microphones were arranged with twelve on a downward arm (azimuth angle ϕ=0^o) and twelve on a sideline arm (azimuth angle ϕ=60^o). Fig. 5a depicts the configuration of the downward arm; the sideline arm is practically identical. On each arm, the polar angles θ ranged approximately from 20 to 120 deg relative to the jet axis. This arrangement enabled simultaneous measurement of the downward and sideline noise at all the polar angles of interest. For noise source mapping, the 24 microphones were aggregated on a linear array as shown in Fig. 5b. The polar aperture was 27.5 deg, with the first microphone at θ=47.5^o and the last microphone at θ=73.0^o.

The microphones were connected, in groups of four, to six conditioning amplifiers (Bruel & Kjaer, Model 2690-A-0S4). The 24 outputs of the amplifiers were sampled simultaneously, at 250 kHz per channel, by two twelve-channel multi-function data acquisition boards (National Instruments PCI-6143). National Instruments LabView

software was used to acquire the signals. The temperature and humidity inside the anechoic chamber were recorded to enable computation of the atmospheric absorption.

The narrowband sound pressure level spectra were corrected for actuator response, free-field correction, and atmospheric absorption. Overall sound pressure levels (OASPL) were obtained by integrating the corrected spectra. The conditions used for EPNL calculations in the downward and sideline directions are shown in Fig.6 and reflect the typical takeoff profile for the HWB. The microphone measurements in the downward (ϕ=0^o) and sideline (ϕ=60^o) directions were used respectively to assess the downward and sideline EPNL. Details of the PNL and EPNL calculation procedure can be found in Ref. 5. The reduction in EPNL (ΔEPNL) is used as a preliminary "figure of merit" in the assessment of jet noise shielding.

Noise source maps of the jets were generated from the deconvolution of the delay-and-sum beamforming output of the microphone array (Fig. 5b). The method is based broadly on the DAMAS approach of Brooks and Humphreys[8] with additional features for self-consistent imaging of directional sources developed by Papamoschou[9]. Deconvolution utilized the Richardson-Lucy inversion method[9,10].

C. Mean flow testing

For mean velocity measurements, the nozzles were attached to a duplicate dual-stream apparatus. Compressed air was supplied to both the primary (core) and secondary (bypass) nozzles at room temperature. The exit conditions were M_p=0.900, U_p=286 m/s, M_s=0.625, and U_s=206 m/s. Even though the velocities were lower than those of a realistic turbofan exhaust (reproduced in the acoustic tests), the velocity ratio U_s/U_p=0.72 matched the velocity ratio in the acoustics tests. The Reynolds number of the jet, based on fan diameter, was 0.54×10^6.

The mean velocity field in the jet plume was measured using a Pitot rake system, shown in Fig.7. The rake consists of five 0.5-mm internal diameter probes attached to a motorized three dimensional traverse system. The 70-mm long probes are spaced 10 mm apart and mounted on a streamlined holder. Each Pitot probe is connected individually to a Setra Model 207 pressure transducer. The pressure was sampled at a rate of 1000 Hz by an analog to digital data acquisition board (National Instruments PCI-MIO-16E). Mach number and velocity profiles were computed from the Pitot measurements under the assumptions of constant static pressure (equal to ambient pressure) and constant total temperature (equal to room temperature). Smoothing of the velocity profiles used a Savitzky-Golay filter[11].

III. Results

A. Acoustics surveys

For selected nozzle/shield configurations we present an "acoustic summary" comprising the following quantities: narrowband lossless spectra, scaled to full-scale frequency (scale factor of 90), at selected polar angles; directivity of OASPL; PNL versus time; PNL versus observer polar angle; and estimate of EPNL. These quantities are compared against their respective baseline values (red curves). We begin with the acoustics of the free jets, followed by the acoustics of the jets in combination with the shield.

Free jets

The acoustic effects of the mild chevrons are depicted in Fig. 8. The chevrons reduce modestly the sound pressure level at low frequency. Slight cross-over at high frequency is noted at low polar angles. The estimated EPNL benefit is very small at about 0.2 dB. The aggressive chevrons, Fig.9, produce larger reductions at low frequency but significant excess noise at high frequency. The OASPL reduction is quite strong, approximately 3 dB, but it is primarily due to reductions at low frequency. As a result, the EPNL benefit is a modest 0.4 dB. The results for wedge W18x3 are presented in Fig. 10 for the sideline and downward directions. In the downward direction there is substantial noise reduction in low and mid frequencies, with no crossover at high frequency. As a result, the downward EPNL reduction is significant at 1.7 dB. In the sideline direction the trends are somewhat weaker, with slight crossover at large polar angles, resulting in an EPNL reduction of 0.7 dB. The combination of aggressive chevrons and wedge, Fig. 11, produces large OASPL reduction but weaker EPNL benefit due to appreciable crossover caused by the chevrons.

Shielded jets

We compare the acoustics of shielded jets with the acoustics of the plain unshielded nozzle. This gives an assessment of the overall benefit of shielding. Shielding of the plain nozzle, Fig. 12, produces benefits only at large polar angles and high frequency. The EPNL benefit is modest at 1.1 dB downward and 1.3 dB sideline. With application of the mild chevrons, Fig. 13, we note improvement in shielding at aft angles. The EPNL benefit increases moderately to 1.8 dB downward and 1.7 dB sideline. The aggressive chevrons, Fig. 14, improve the

acoustic performance substantially. We note reduction at all polar angles, with very strong attenuation at large polar angles. Crossover at small polar angles is caused primarily by the excess noise of the chevrons at high-frequency. The EPNL benefit of the shielded aggressive-chevron nozzle (again, with respect to the plain unshielded nozzle) is estimated at 3.3 dB downward and 3.1 dB sideline. The wedge deflector W18x3, Fig.15, is also very effective at producing large noise attenuations. The downward EPNL benefit of 3.9 dB is due in part to the noise suppression of the wedge itself (Fig. 10) as well as the shielding. The sideline benefit of 3.0 dB is primarily the effect of the shielding. The combination aggressive wedge and shield, Fig. 16, combines features from the individual components but the improvement is marginal. The significant cross-over at small polar angles offsets somewhat the very large reductions at large polar angles.

Our study included seven additional porous wedge deflectors as well as a combination of wedge with mild chevrons. The detailed acoustics are omitted here for brevity. Table 3 lists the estimated EPNL reductions. Out of this optimization process the wedge W18x3 emerged as the best stand-alone device for improving shielding. The combination of wedge and mild chevrons did not provide any benefit relative to the wedge alone.

B. Noise source distributions

The deconvolution procedure of Ref. 9 yields high-resolution noise source distributions $q(Sr, x/D_s)$. They are presented here in the normalized form $q(Sr, x/D_s)/q_{max}(Sr)$ that helps identify the location of peak noise versus frequency. It is instructive to connect each noise source distribution to the corresponding map of insertion loss. The insertion loss is defined as the reduction in sound pressure level, for a particular nozzle, caused by the shield. In other words, we compare the free chevron nozzle to the chevron nozzle with shield, and so on. The insertion loss is plotted against Strouhal number and polar angle.

Figure 17 presents noise source distributions and insertion-loss maps for the plain nozzle and the two chevron configurations. For the plain nozzle, the peak noise source location is practically constant at x/D_s=4.0 up to Sr=6, then it drops abruptly to x/D_s=−1 (it should be kept in mind that x is defined relative to plug tip, so x/D_s=−1 denotes the fan exit plane). This sudden transition has been observed in the past in phased array measurements of full-scale high-bypass turbofan engines[12]. The insertion loss map shows very small values except at high polar angles. Examining the insertion loss at θ =100 deg, for example, we see modest levels until the Strouhal number rises to about 6, above which the level becomes significant. The large insertion loss at high frequency is associated with the noise source moving upstream near the fan exit plane. The mild chevrons produce modest changes to the noise source distribution, lowering the transition Strouhal number to Sr≈4.5 and correspondingly increasing moderately the insertion loss levels at large angles. Application of the aggressive chevrons makes a notable change in the noise source location, moving the transition Strouhal number to Sr≈1.2. The insertion loss map shows very significant levels starting at Sr≈1.2.

Related results for the wedge W18x3 and combination AC+W18x3 are shown in Fig.18. In contrast to the abrupt transition in the peak noise source location with the chevrons, the wedge induces a more gradual trend of reduction in noise source length. The reduction is significant but not as large as with the aggressive chevrons. As a result, the insertion loss levels are somewhat lower than those achieved with the chevrons. The combination AC+W18x3 offers moderately larger noise source compaction than the aggressive chevrons alone.

It is evident from these results that the aggressive chevrons offer the largest noise source compaction and resulting insertion loss. However, the aggressive chevrons, by themselves, are noisy at high frequency, as seen in the spectral plots of Fig. 9. This offsets somewhat the insertion loss benefit. The insertion loss of the wedge is more modest, but the wedge is inherently quieter than the aggressive chevrons. For this reason, the wedge has a small overall acoustic benefit over the chevrons, as seen in Table 3.

C. Mean velocity

Contours of the mean axial velocity on the symmetry plane (z=0) are plotted in Fig.19 for five of the jets investigated. The high-speed region (u>0.9U_p) of the jet from the plain nozzle extends to about 3.5 fan diameters D_s from the plug tip, x/D_s=3.5. The mild chevrons cause the counter-intuitive effect of moderately elongating the high-speed region to x/D_s=4.0. The aggressive chevrons do not change appreciably the length of the high-speed region but reduce its volume. The wedge imparts asymmetry to the flow field, with the low-speed region on the base of the wedge evident, and reduces the length of the high-speed region to x/D_s=2.9. The combination of wedge and aggressive chevrons leads to further contraction of the high-speed region to x/D_s=2.5.

Cross-sectional cuts of the axial mean velocity are shown in Fig.20 for the near field. The plain nozzle presents a very axisymmetric pattern indicating good alignment of its components. The mild and aggressive chevrons impact the mean velocity pattern only for x/D_s <1; downstream, the pattern becomes circular as in the plain case. The

wedge concentrates fan flow in the downward direction, with the wake evident in the top region; its effect persists longer than the effects of the chevrons.

The axial distribution of the local maximum velocity $u_{max}(x)$ is plotted in Fig. 21. The mild chevrons elongate moderately the high-speed region and reduce the velocity decay past x/D_s =3.5. The aggressive chevrons induce a small reduction in u_{max} in the near field but also reduce the decay rate for x/D_s >3.5. In contrast, the wedge W18x3 causes an appreciable contraction of the high-speed region and does not alter significantly the downstream decay rate. The combination of aggressive chevrons and wedge reduces even further the high-speed region.

Although the compaction of the high speed region by the wedge could be connected to the alteration of the noise source map seen in Fig.18, the same is not true for the chevrons. For the aggressive chevrons there is no straight-forward way to connect the mean velocity field, whose high-speed length did not change, to the dramatic reduction of noise source length at high frequency seen in Fig. 17. It is apparent that, for these complex flows, the mean velocity field alone does not provide enough information to infer a noise source length.

IV. Conclusions

We addressed in subscale experiments the problem of shielding of jet noise from a high-bypass nozzle by a shield shaped in the form of a generic Hybrid Wing Body airplane. Redistribution of the jet noise source is essential for achieving substantial noise reduction. Devices used to alter the jet noise source comprised chevrons (in mild and aggressive configurations) and a number of porous wedge fan flow deflectors. Using the estimated cumulative (downward plus sideline) EPNL reduction as a figure of merit, shielding of the plain nozzle yielded a 2.5 dB reduction. Application of the aggressive chevrons increased the reduction to 6.5 dB, while the best wedge configuration improved this figure to 6.9 dB. Combination of wedge and aggressive chevrons yielded a benefit of 7.6 dB.

Examination of high-definition noise source maps shows a direct link between insertion loss and axial location the peak noise. There are differences in the ways the nozzle devices change the location of the peak noise source. The aggressive chevrons cause an abrupt contraction at Strouhal number Sr=1.2, while the wedge induces a gradual contraction with increasing frequency. As a result, the insertion loss with the aggressive chevrons is stronger than with the wedge. However, because the wedge is inherently quieter than the chevrons, it gives a slightly better overall benefit.

Surveys of the mean flow field show that the wedge, and its combination with chevrons, produces a significant reduction in the potential core length. On the other hand, the chevrons alone induce modest changes in the length of the high-speed region of the jet. Therefore, the mean velocity field by itself cannot provide useful information for inferring the noise source location for these complicated flows. It is possible that turbulent kinetic energy distributions, most likely generated by computations, will be useful in this regard.

Acknowledgment

This research has been funded by Boeing Subcontract No. 208547 in support of NASA contract NNL07AA54C "Acoustic Prediction Methodology and Test Validation for an Efficient Low-Noise Hybrid Wing Body Subsonic Transport." We thank Dr. Eric Unger (Boeing) for his design of the chevron nozzles.

References

1. Von Glahn, U., Groesbeck, D., and Reshotko, M. "Geometry Considerations for Jet Noise Shielding with CTOL Engine-Over-The-Wing Concept," AIAA Paper 74-568, June 1974.
2. Von Glahn, U., Goodykoontz, J., and Wagner, J. "Nozzle geometry and forward velocity effects on noise for CTOL engine-over-the-wing concept," NASA TM-X-71453, Oct. 1973
3. Von Glahn, U., Groesbeck, and D. Wagner, J., "Wing shielding of high-velocity jet and shock-associated noise with cold and hot flow jets," AIAA Paper 76-547, July 1976.
4. Liebeck, Robert H., "Design of the Blended Wing Body Subsonic Transport," *Journal of Aircraft*, Vol. 41, No. 1, January–February 2004.
5. Papamoschou, D., and Mayoral, S., "Experiments on Shielding of Jet Noise by Airframe Surfaces," AIAA-2009-3326, May 2009.
6. Papamoschou, D., "Pylon Based Jet Noise Suppressors," *AIAA Journal*, Vol. 47, No.6, 2009, pp. 1408-1420.
7. Papamoschou, D., "Acoustic Simulation of Coaxial Hot Air Jets Using Cold Helium-Air Mixture Jets," *Journal of Propulsion and Power*, Vol. 23, No.2, 2007, pp. 375-381.
8. Brooks, T.F., and Humphreys, W.M., "A Deconvolution Approach for the Mapping of Acoustic Sources (DAMAS) Determined from Phased Microphone Arrays," AIAA-2004-2954, May 2004
9. Papamoschou, D., "Imaging of Distributed Directional Noise Sources," AIAA-2008-2885, May 2008.

10. Richardson, W.H., "Bayesian-Based Iterative Method of Image Restoration," *Journal of the Optical Society of America*, Vol. 62, No. 1, 1972, pp. 55-.
11. Savitzky, A. and Golay, M.J.E. "Smoothing and Differentiation of Data by Simplified Least Squares Procedures," Analytical Chemistry, Vol. 36, No. 8, 1964, pp. 1627-.
12. Brusniak, L., Underbrink, J.R., and Nesbitt, E., "Phased Array Measurements of Full-Scale Exhaust Noise," AIAA Paper 2007-3612, May 2007.

Table 1 Geometry of porous wedges

Wedge	Half-angle (deg)	Height (mm)	Distance of apex from fan exit plane (mm)
W15	15	5	0
W18	18	5	0
W21	21	5	0
W30	30	5	0
TW15	15	7	0
TW18	18	7	0
W18x3	18	5	3
TW18x3	18	7	3

All wedges had solidity of 49.6% and side length = 13 mm. Fan exit height = 4 mm.

Table 2 Cycle conditions for the BPR10 Nozzle

Quantity	Core	Fan
NPR	1.376	1.550
NTR	2.950	1.139
T_0 (K)*	864	334
T (K)*	781	291
M	0.691	0.817
U (m/s)	387	279

*Equivalent conditions using helium-air mixture jets

Table 3 EPNL reductions

Case	EPNL reduction (dB) relative to unshielded modified nozzle		EPNL reduction (dB) relative to unshielded plain nozzle		
	Downward	Sideline	Downward	Sideline	Down+Side
B	1.07	1.29	1.07	1.29	2.36
MC	1.61	1.43	1.85	1.72	3.57
AC	2.96	3.11	3.34	3.15	6.49
W18x3	2.16	2.34	3.86	3.05	6.91
AC+W18x3	3.22	3.26	4.32	3.30	7.62
W15	1.72	1.47	3.24	2.12	5.36
W18	2.21	2.17	3.91	2.28	6.19
W21	2.04	1.68	3.85	1.96	5.81
W30	3.09	3.59	3.83	2.40	6.23
TW15	1.72	1.43	3.58	1.78	5.36
TW18	1.91	1.56	3.95	1.63	5.58
TW18x3	1.97	1.33	4.04	2.29	6.33
MC+W18x3	2.27	2.22	3.97	2.48	6.45

B: baseline
MC: mild chevrons
AC: aggressive chevrons
Wxx and TWxx: perforated wedge with half angle xx-degrees (Table 1)

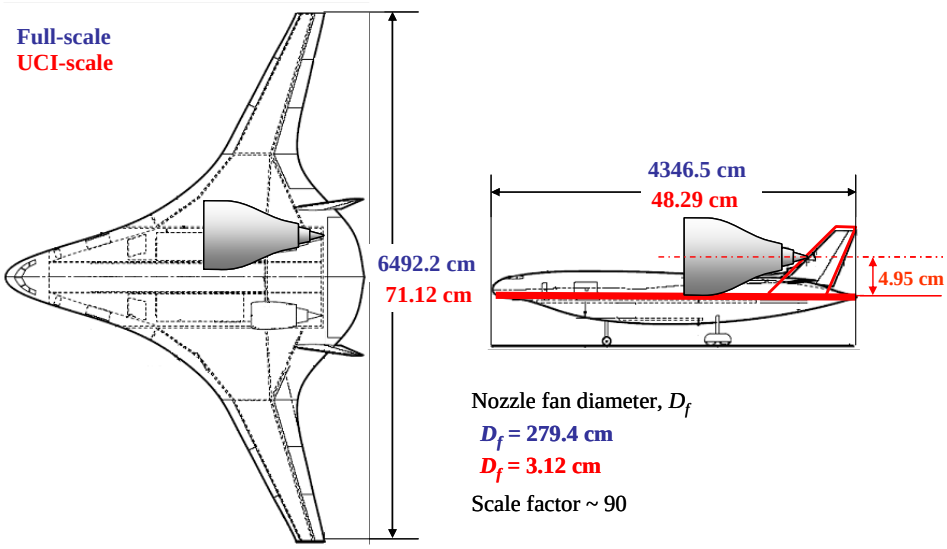

Fig. 1 Scaling of HWB planform to UCI dimensions and retention of critical dimensions for shielding (red lines).

Fig. 2 Installation of nozzle and HWB shield.

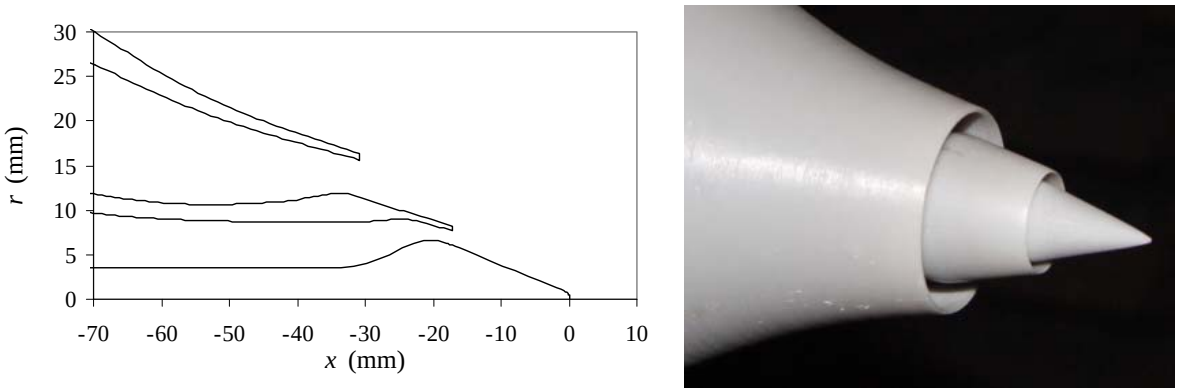

Fig. 3 Coordinates and picture of BPR10 nozzle

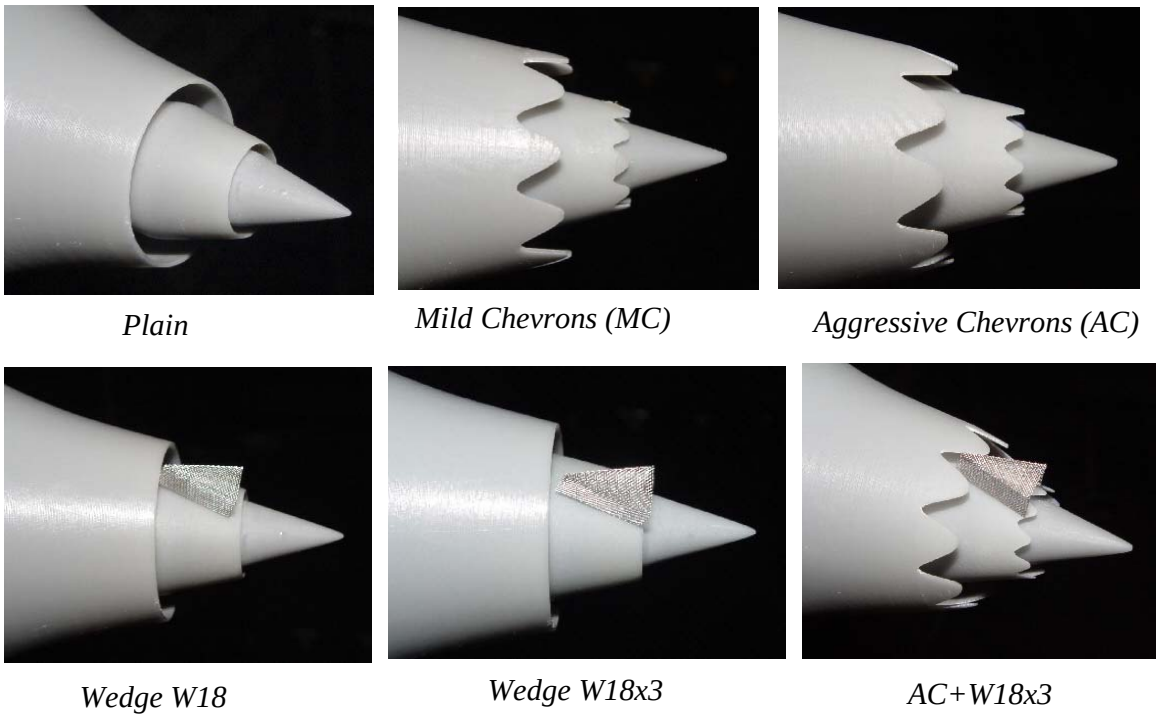

Fig. 4 Subset of the nozzle configurations tested

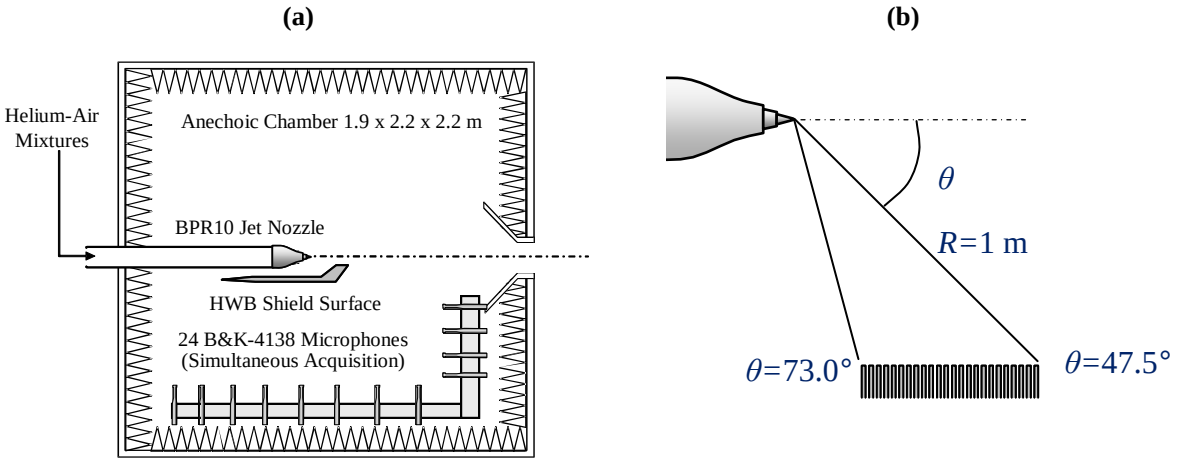

Fig. 5 Aeroacoustic measurement. (a) Setup for acoustic surveys; (b) setup for noise source imaging.

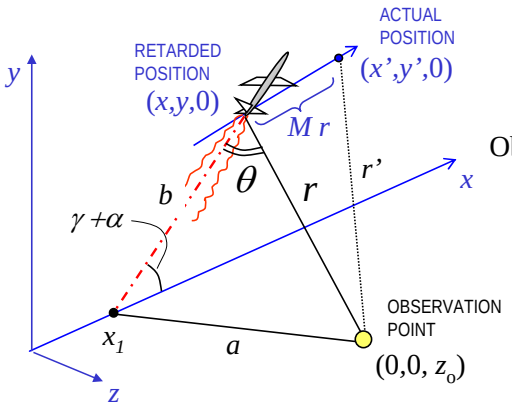

Aircraft flying with Mach number M, angle of attack α, and climb angle γ

Observation distance and polar emission angle

$$r' = \sqrt{(x'-x_o)^2 + y'^2 + z_o^2}$$

$$r = \sqrt{(x-x_o)^2 + y^2 + z_o^2}$$

$$\tan(\theta/2) = \sqrt{\frac{(p-b)(p-r)}{p(p-a)}}$$

where

$$x_1 = x - y/\tan(\gamma+\alpha)$$

$$a = \sqrt{(x_o - x_1)^2 + z_o^2}$$

$$b = y/\sin(\gamma+\alpha)$$

$$p = \frac{1}{2}(a+b+r)$$

CONDITIONS FOR EVALUATON OF PNL		
	SIDELINE	DOWNWARD
Lateral distance, z_o=	1476 ft	0 ft
Altitude at x=0	1000 ft	1500 ft
Angle of attack, α=	12 deg	10 deg
Climb angle, γ=	10 deg	4 deg
Flight Mach, M=	0.20	0.30

Fig. 6 Geometric relations and conditions for assessment of perceived noise level.

(a) **(b)**

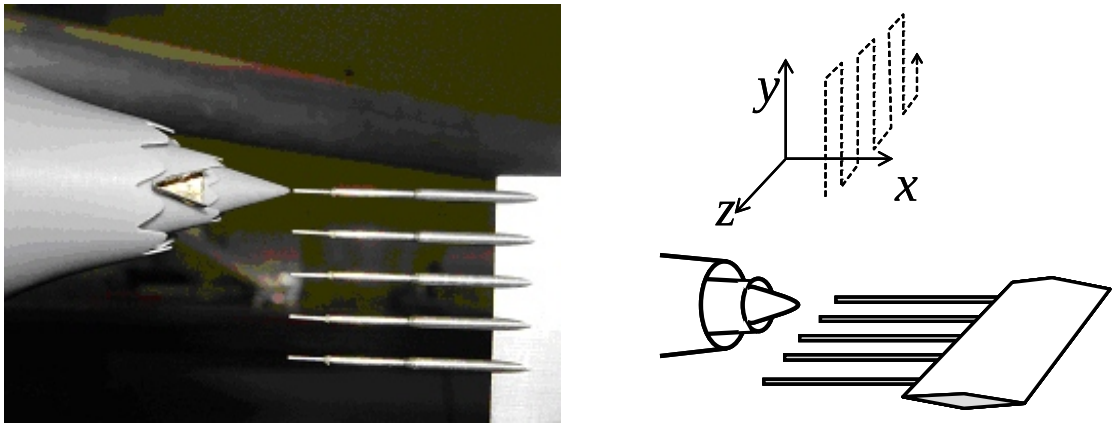

Fig. 7 Instrumentation for mean flow surveys. (a) Pitot rake; (b) scan pattern for each axial position.

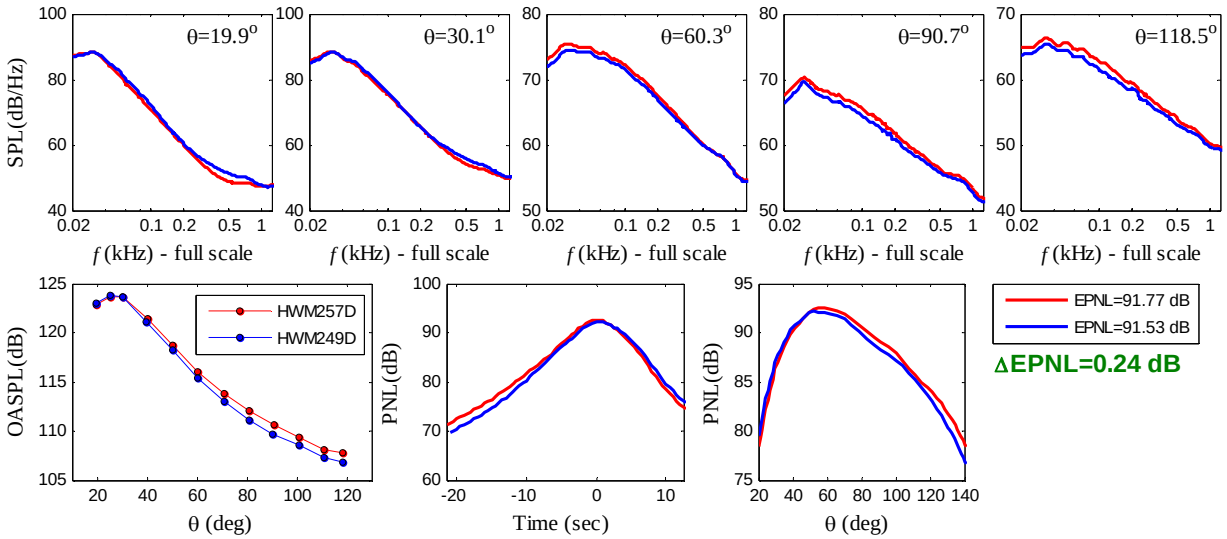

Fig. 8 Acoustics of jets without shield. Mild chevrons (blue) compared to plain nozzle (red).

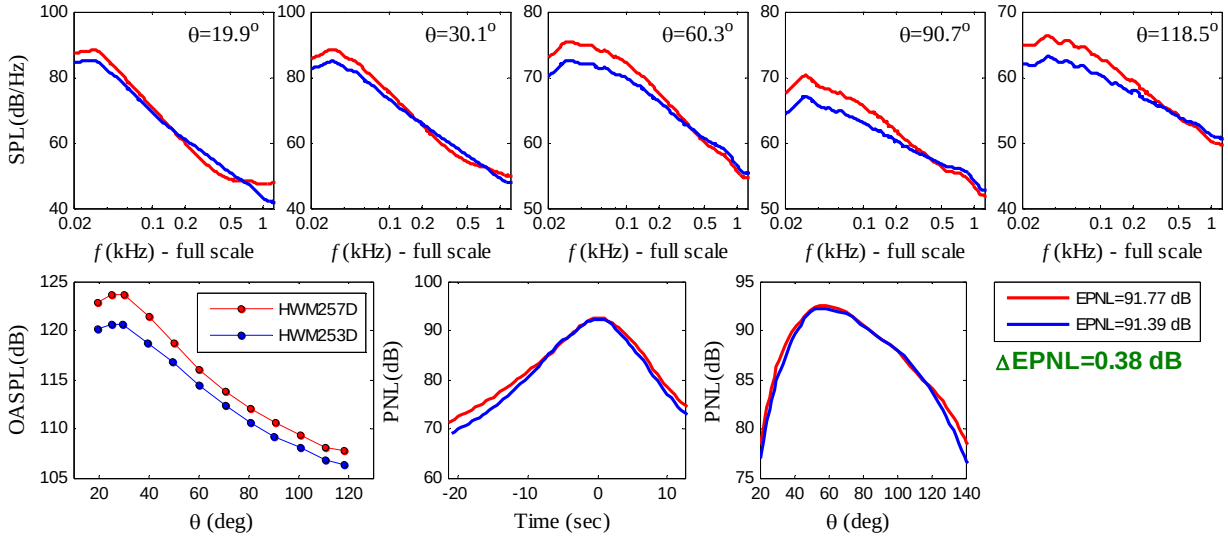

Fig. 9 Acoustics of jets without shield. Aggressive chevron nozzle (blue) compared to plain nozzle (red).

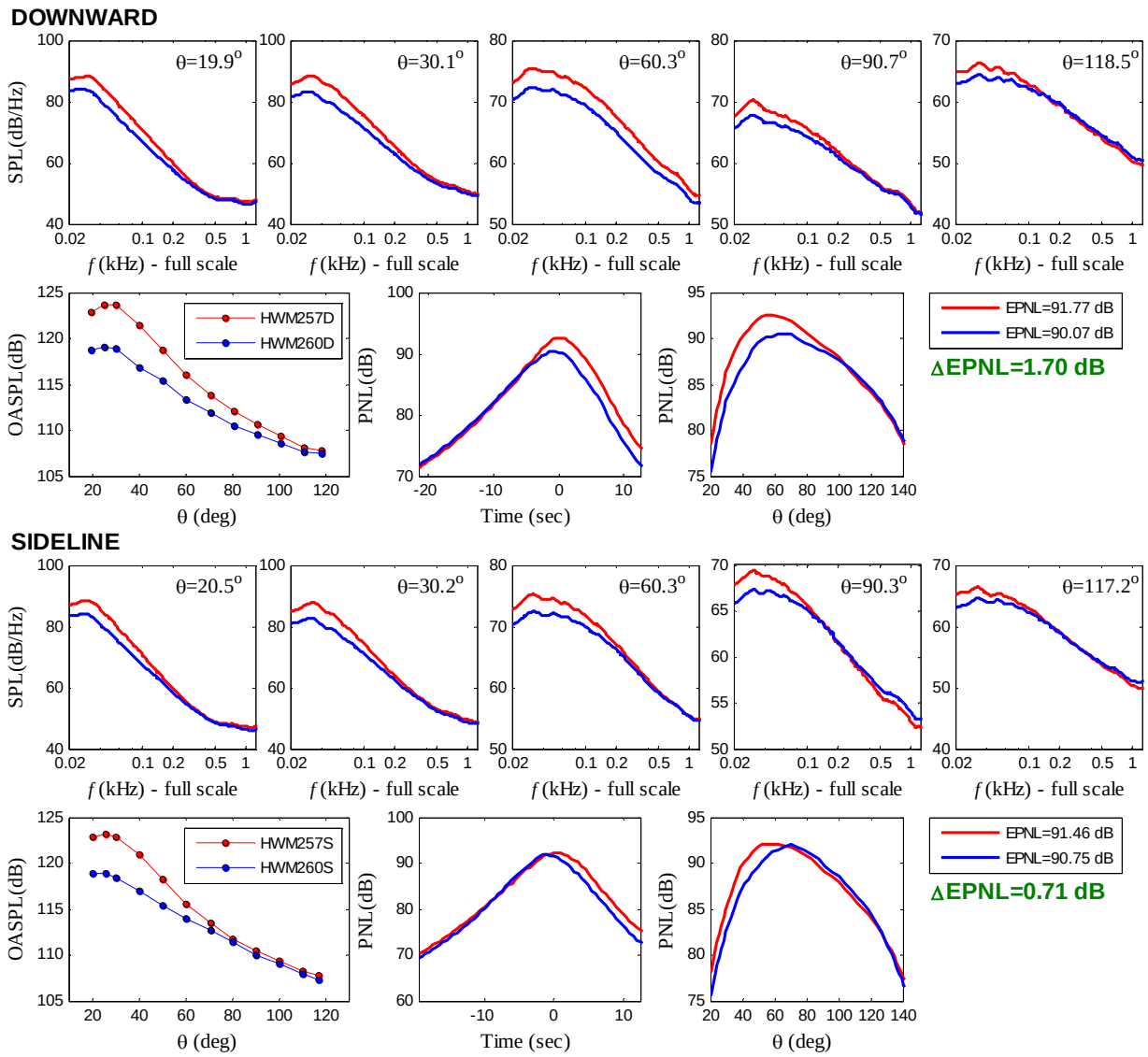

Fig. 10 Acoustics of jets without shield. Wedge W18x3 nozzle (blue) compared to plain nozzle (red).

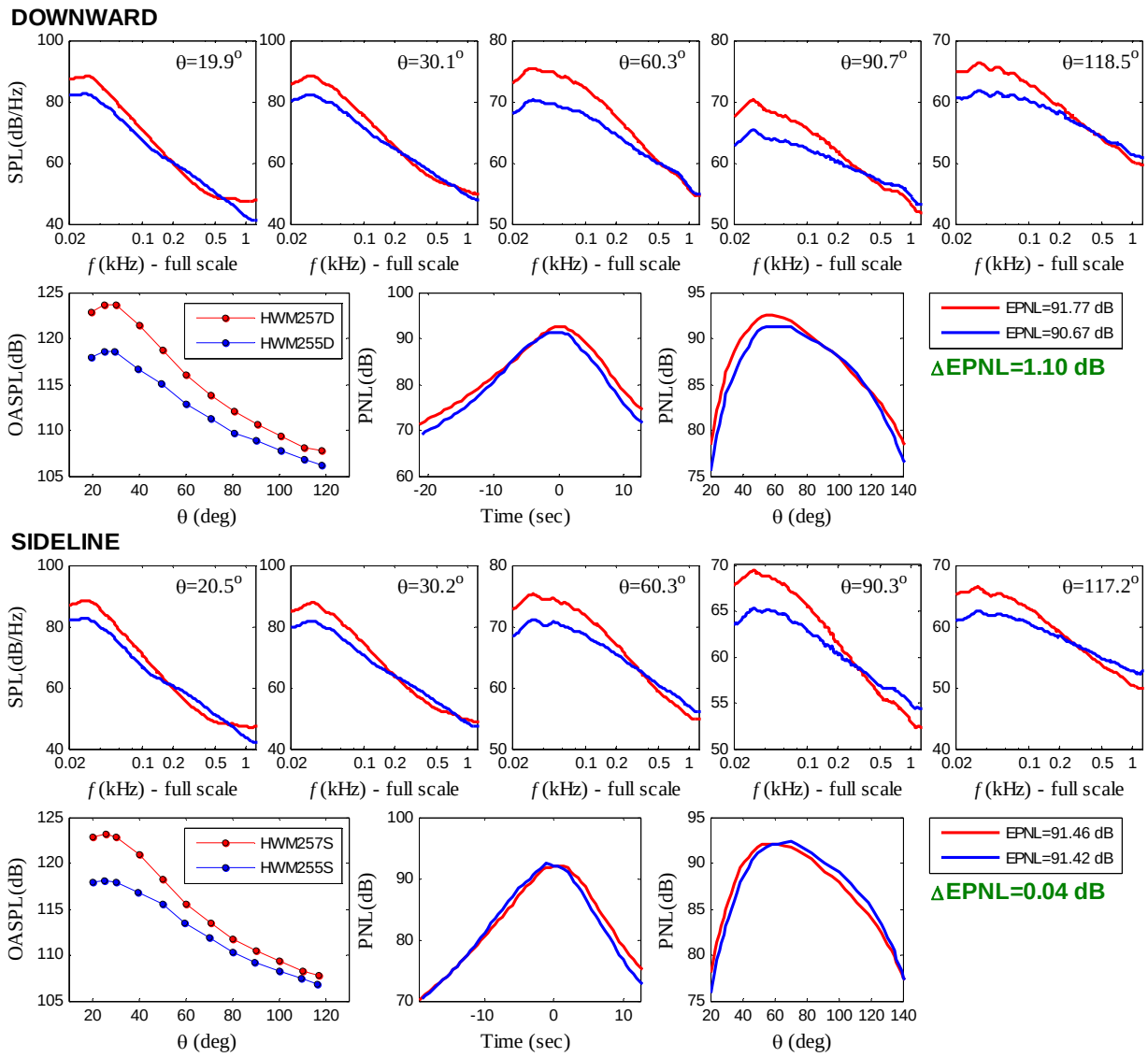

Fig. 11 Acoustics of jets without shield. Combination AC+W18x3 nozzle (blue) compared to plain nozzle (red).

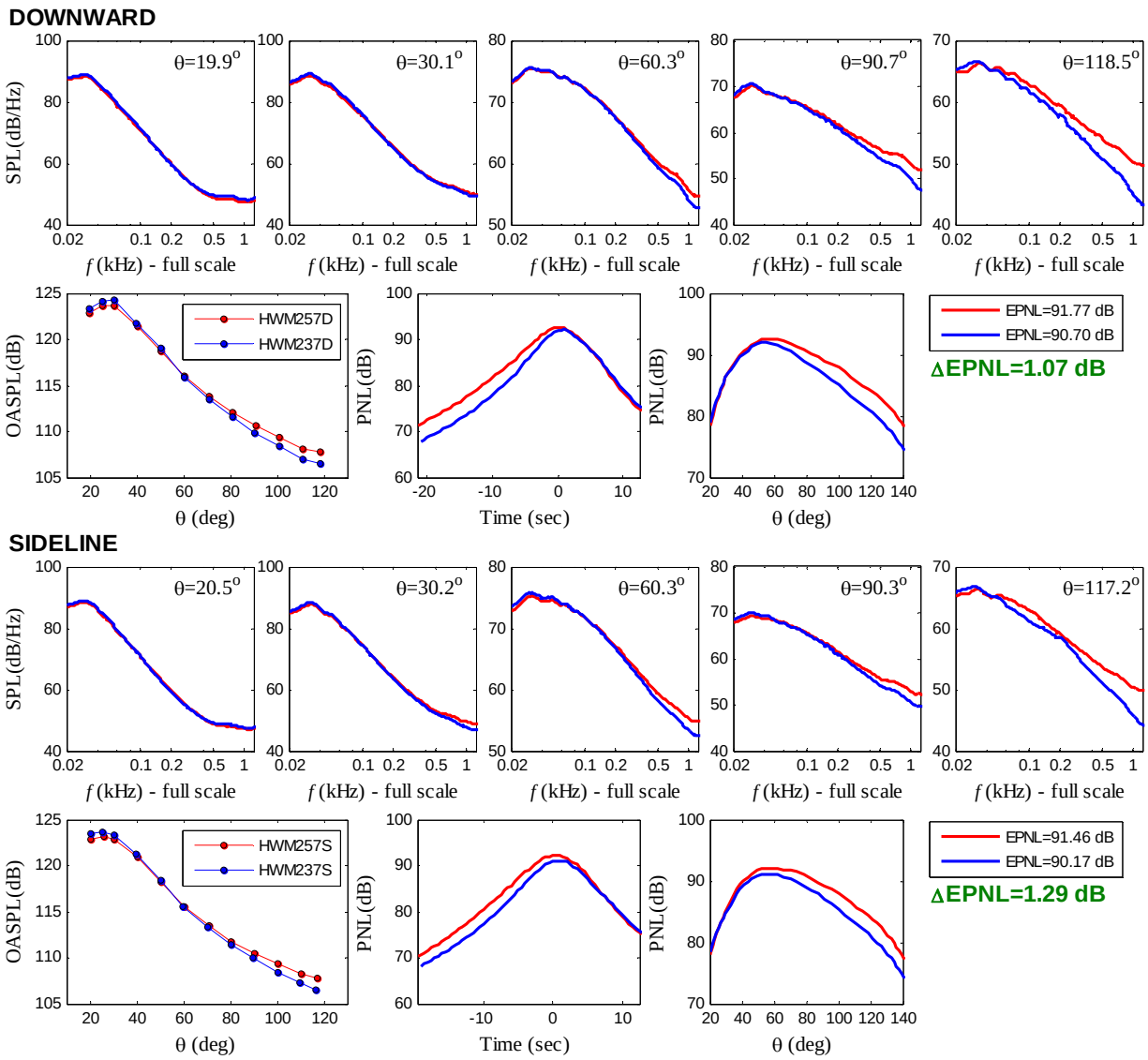

Fig. 12 Effect of shield on acoustics. Shielded plain nozzle (blue) compared to unshielded plain nozzle (red).

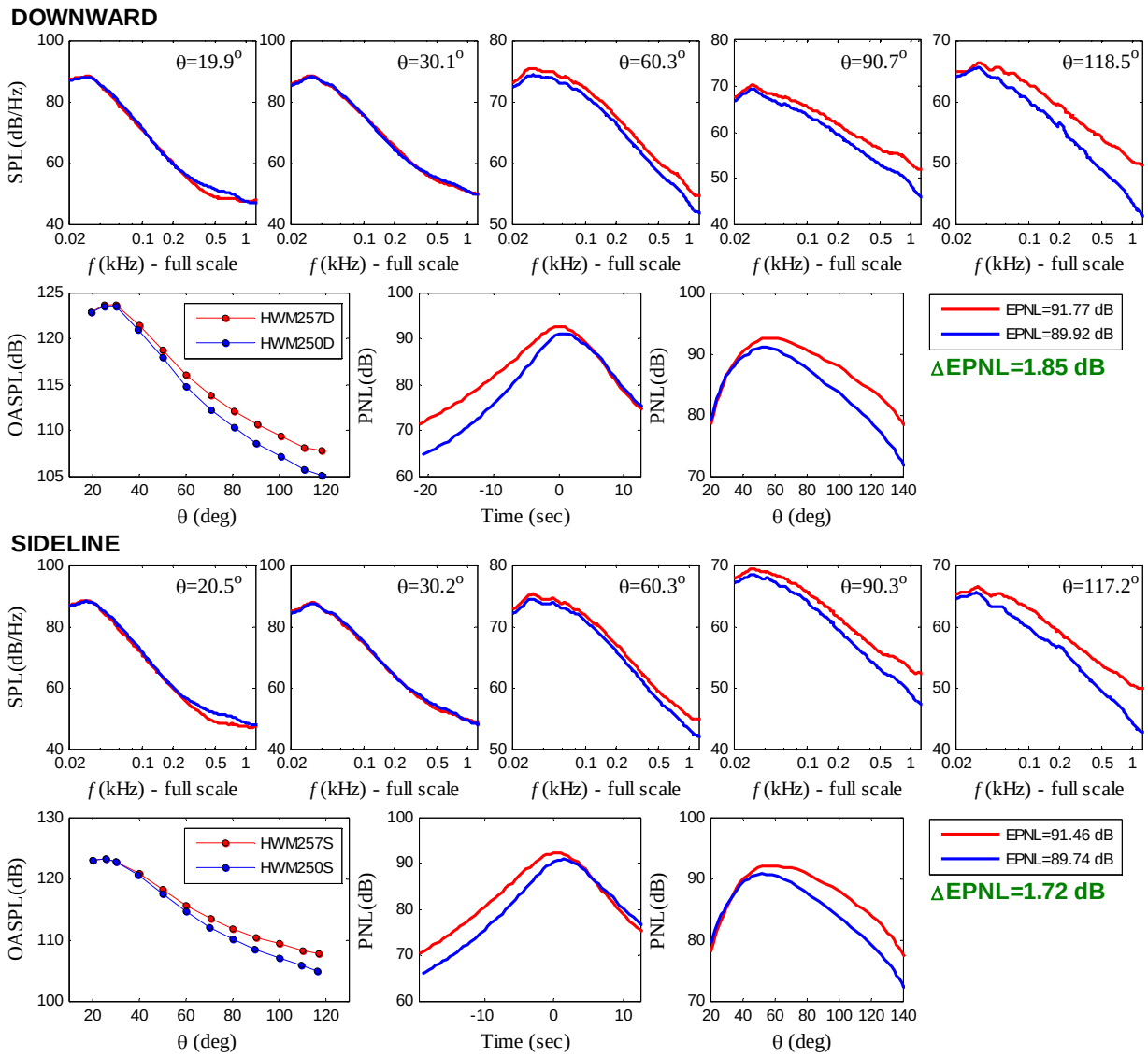

Fig. 13 Effect of shield on acoustics. Shielded mild chevron nozzle (blue) compared to unshielded plain nozzle (red).

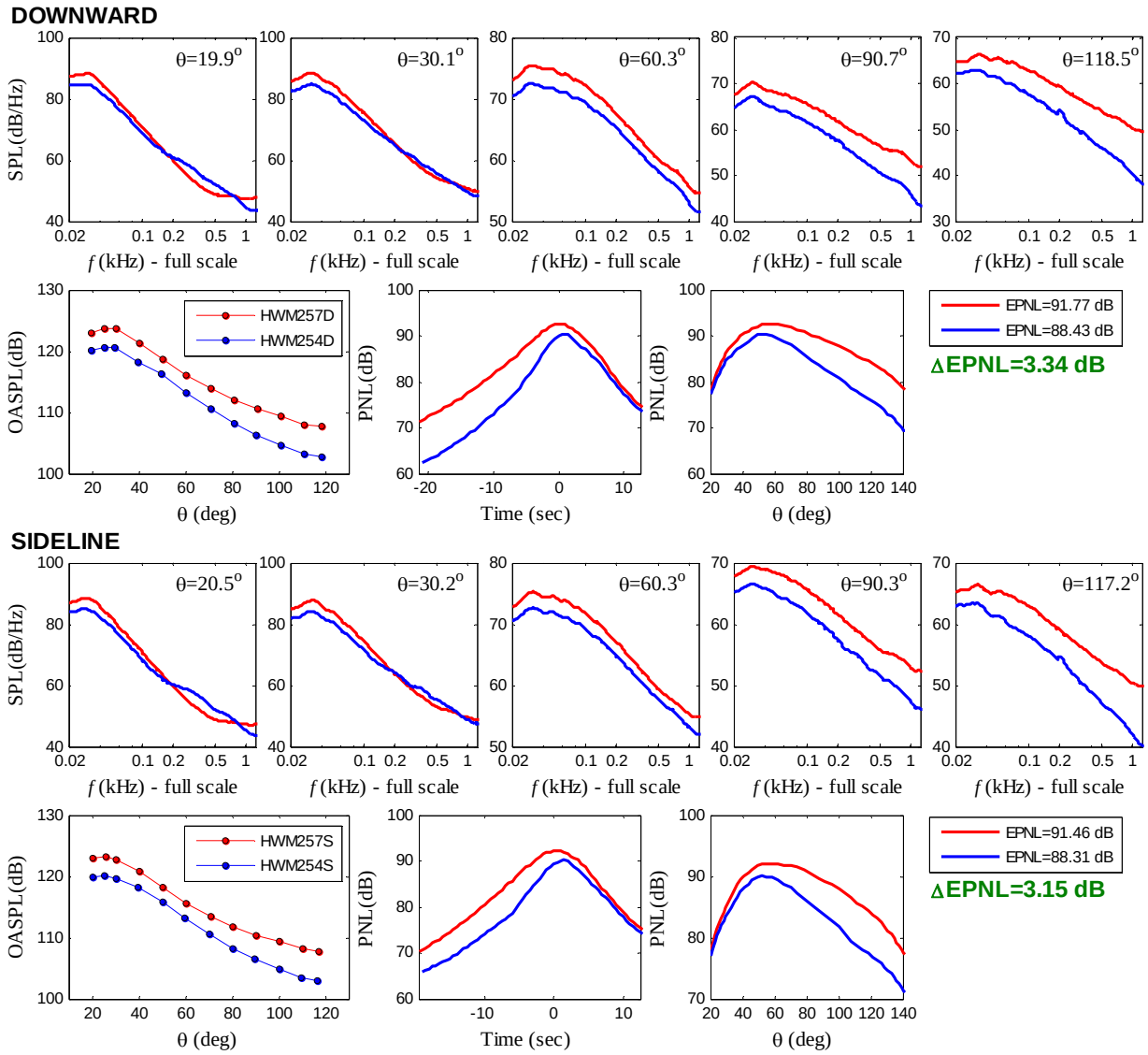

Fig. 14 Effect of shield on acoustics. Shielded aggressive chevron nozzle (blue) compared to unshielded plain nozzle (red).

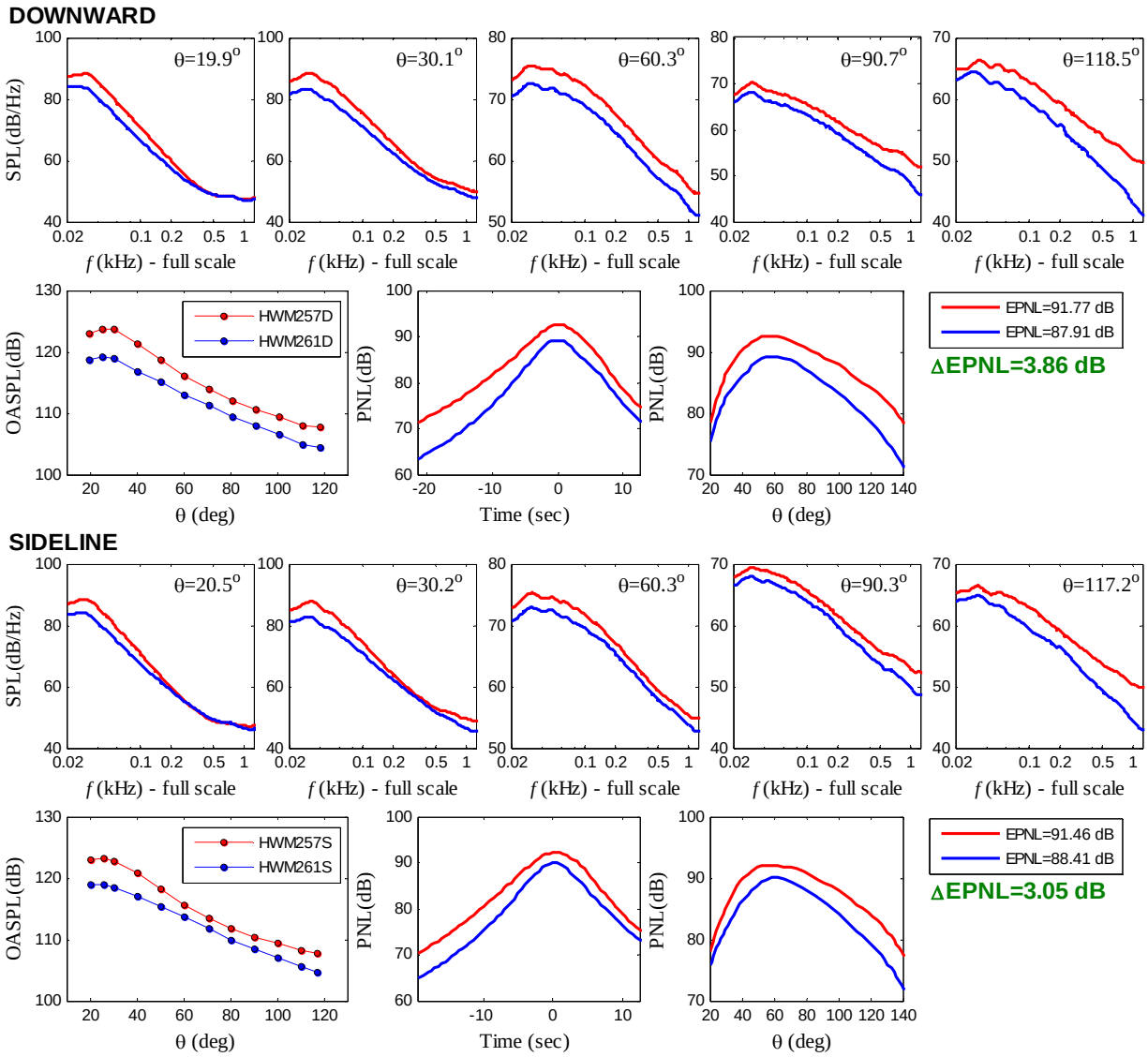

Fig. 15 Effect of shield on acoustics. Shielded wedge W18x3 nozzle (blue) compared to unshielded plain nozzle (red).

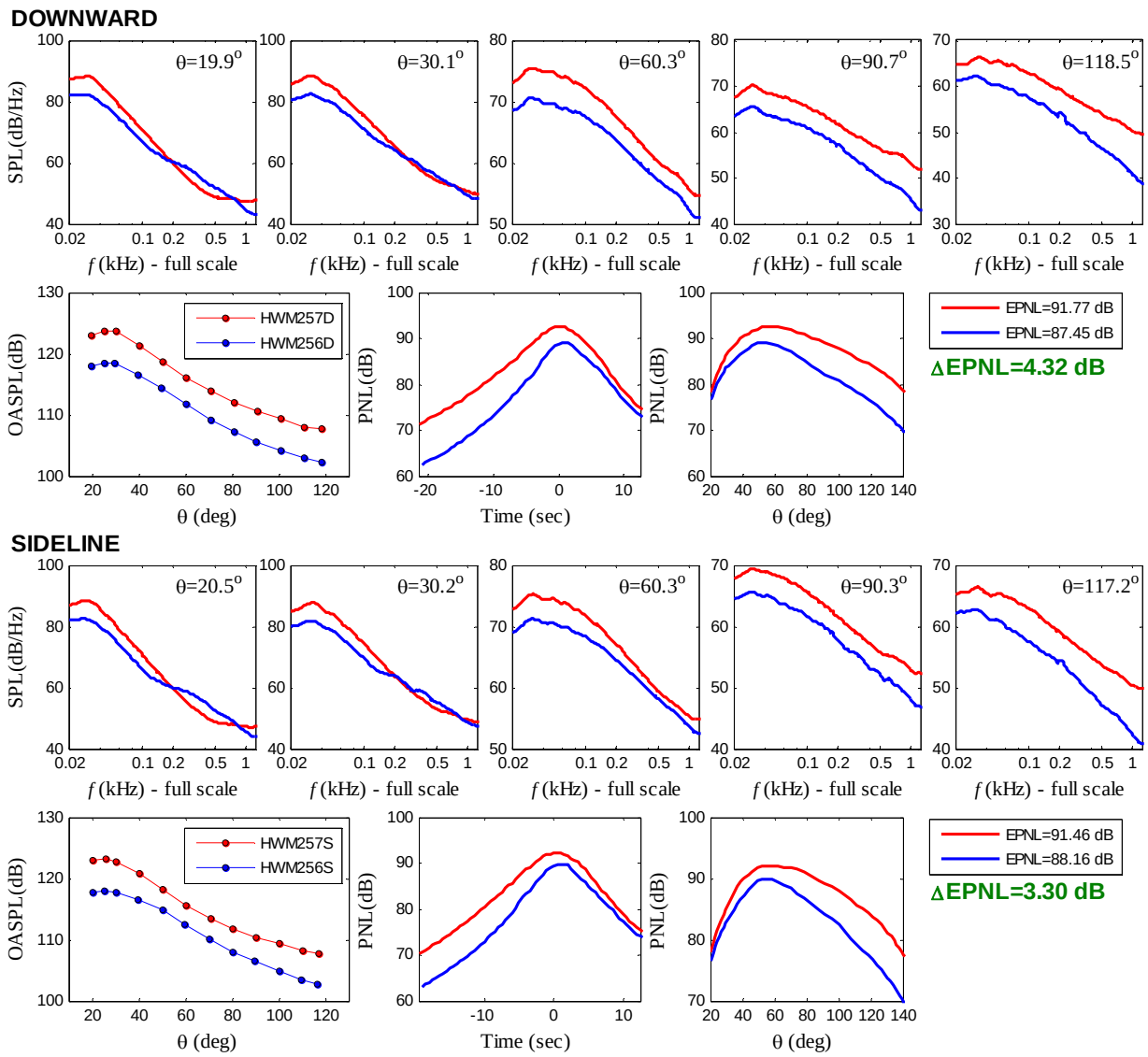

Fig. 16 Effect of shield on acoustics. Shielded AC+W18x3 nozzle (blue) compared to unshielded plain nozzle (red).

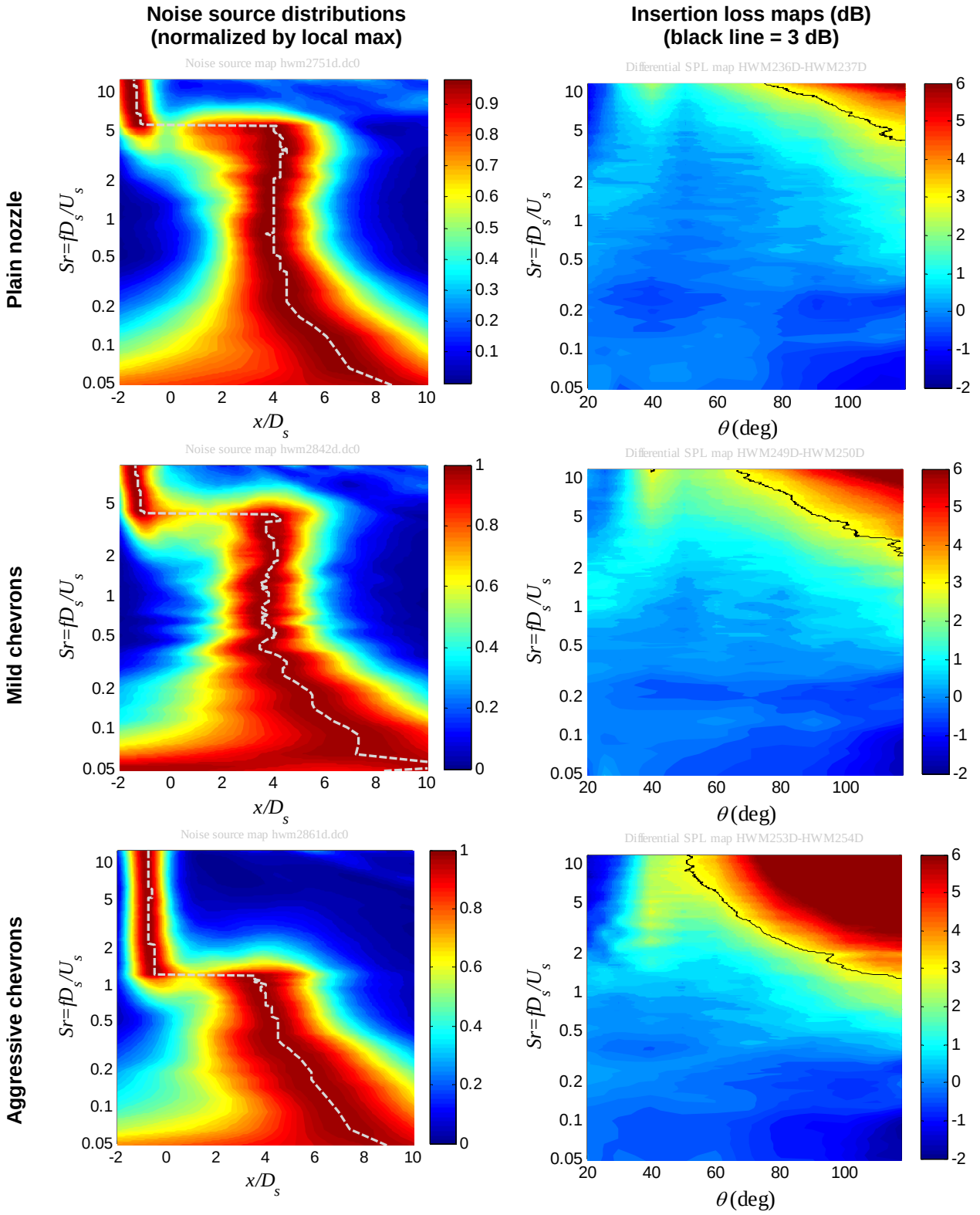

Fig. 17 Left column: Noise source distribution for unshielded jets; dashed white line indicates location of peak noise. Right column: Corresponding insertion loss maps with application of shield. Results shown for plain nozzle, mild chevrons and aggressive chevrons.